Characterization of the Zinc Sites in Cobalamin-Independent and Cobalamin-Dependent Methionine Synthase Using Zinc and Selenium X-ray Absorption Spectroscopy†

Katrina Peariso,‡ Zhaohui S. Zhou,§ April E. Smith,|| Rowena G. Matthews,*,§ and James E. Penner-Hahn*,‡

Department of Chemistry, Biophysics Research Division and Department of Biological Chemistry, and Interdepartmental Program in Medicinal Chemistry, The University of Michigan, Ann Arbor, Michigan 48109-1055

Received July 24, 2000; Revised Manuscript Received November 2, 2000

ABSTRACT: X-ray absorption spectroscopy has been used to investigate binding of selenohomocysteine to cobalamin-independent (MetE) and cobalamin-dependent (MetH) methionine synthase enzymes of *Escherichia coli*. We have shown previously [Peariso et al. (1998) *J. Am. Chem. Soc. 120*, 8410−8416] that the Zn sites in both enzymes show an increase in the number of sulfur ligands when homocysteine binds. The present data provide direct evidence that this change is due to coordination of the substrate to the Zn. Addition of L-selenohomocysteine to either MetE or the N-terminal fragment of MetH, MetH(2−649), causes changes in the zinc X-ray absorption near-edge structure that are remarkably similar to those observed following the addition of L-homocysteine. Zinc EXAFS spectra show that the addition of L-selenohomocysteine changes the coordination environment of the zinc in MetE from 2S + 2(N/O) to 2S + 1(N/O) + 1Se and in MetH(2−649) from 3S + 1(N/O) to 3S + 1Se. The Zn−S, Zn−Se, and Se−S bond distances determined from the zinc and selenium EXAFS data indicate that the zinc sites in substrate-bound MetE and MetH(2−649) both have an approximately tetrahedral geometry. The selenium edge energy for selenohomocysteine shifts to higher energy when binding to either methionine synthase enzyme, suggesting that there is a slight decrease in the effective charge of the selenium. Increases in the Zn−Cys bond distances upon selenohomocysteine binding together with identical magnitudes of the shifts to higher energy in the Se XANES spectra of MetE and MetH(2−649) suggest that the Lewis acidity of the Zn sites in these enzymes appears the same to the substrate and is electronically buffered by the Zn−Cys interaction.

Catalytic roles for zinc are well established in a variety of metalloenzymes. In most of these, the zinc is ligated by nitrogen- and oxygen-containing amino acid side chains and has an open ligation site occupied by a water molecule (*1*). This water molecule can be ionized or polarized to provide hydroxide ions at physiological pH, or it can be displaced by substrate with subsequent Lewis acid activation of the substrate by the zinc ion. Recent studies have discovered a new class of catalytic zinc metalloproteins in which the zinc is ligated primarily by cysteine thiolates (*2*). These metalloproteins catalyze the transfer of an alkyl group to a nucleophilic thiolate substrate. It has been suggested that coordination of the substrate thiol to the zinc ion lowers the pK_a of the thiol, thereby increasing the concentration of thiolate at physiological pH (*3*). However, the detailed mechanism of the alkyl transfer has yet to be determined.

Two recently characterized zinc-containing enzymes that catalyze alkyl transfers to thiol substrates are the cobalamin-independent (MetE)[1] and cobalamin-dependent (MetH) methionine synthases from *E. coli*. These enzymes catalyze methyl transfer from methyltetrahydrofolate (CH_3-H_4folate) to homocysteine to complete the de novo biosynthesis of methionine (*4*). While the two enzymes have no sequence similarity and have different requirements for catalytic activity (*5*), both enzymes contain 1 equiv of zinc per mole of protein (*6*). Moreover, both enzymes require zinc for binding of homocysteine and for catalysis of methyl transfer to the homocysteine thiolate. An N-terminal fragment of MetH, MetH(2−649), includes both substrate domains, but lacks the cobalamin-binding and activation modules. This fragment retains the ability to catalyze methyl transfer to exogenous cob(I)alamin from CH_3-H_4folate. MetH(2−649)

† This research was supported in part by grants from the National Institutes of Health (GM-24908 to R.G.M. and GM-38047 to J.E.P.-H.).

* Correspondence should be addressed to J.E.P.-H. at the Department of Chemistry, The University of Michigan, 930 N. University Ave., Ann Arbor, MI 48109-1055. FAX (734)647-4865; Phone (734)764-7324; E-mail jeph@umich.edu. Correspondence should be addressed to R.G.M. at the Biophysics Research Division, The University of Michigan, 930 N. University Ave., Ann Arbor, MI 48109-1055. FAX (734)764-3323; Phone (734)764-9459; E-mail rmatthew@umich.edu.

‡ Department of Chemistry.

§ Biophysics Research Division and Department of Biological Chemistry.

|| Interdepartmental Program in Medicinal Chemistry.

[1] Abbreviations: MetE, cobalamin-independent methionine synthase; MetH, cobalamin-dependent methionine synthase; CH_3-H_4folate, methyltetrahydrofolate; IPTG, β-D-thiogalactopyranoside; TCEP, tris(carboxyethyl)phosphine; DEAE-Sepharose, diethylaminoethyl-Sepharose; DTT, dithiothreitol; SDS−PAGE, sodium dodecyl sulfate−polyacrylamide gel electrophoresis; SeHcy, L-selenohomocysteine; Hcy, L-homocysteine.

10.1021/bi001711c CCC: $20.00
Published on Web 12/30/2000

also catalyzes methyl transfer from exogenous methylcobalamin to homocysteine, producing cob(I)alamin and methionine (*7*).

Previous EXAFS (extended X-ray absorption fine structure) studies have shown that the zinc ligand environments in MetE (*8*) and MetH(2−649) (*9*) are different. MetE contains two cysteine ligands, shown by site-directed mutagenesis to be Cys726 (*8*) and Cys643 (*10*), while MetH contains three cysteine ligands, Cys310, Cys311 (*2*), and Cys247 (*9*). A third protein-derived ligand in MetE is likely to be His641 (*10*). Addition of the homocysteine substrate to either enzyme results in the loss of one N/O ligand and the addition of a sulfur ligand, consistent with direct binding of the homocysteine sulfur to the zinc. However, MetE contains a total of 7 cysteine residues while MetH(2−649) contains 10 (*4*). Consequently, the earlier results do not preclude the possibility of a conformational change upon homocysteine binding that brings other cysteine residues within binding proximity of the zinc.

To identify the sulfur ligand that coordinates to the zinc on homocysteine binding, we have used selenohomocysteine as the substrate for MetE and MetH(2−649). Since there are no selenium-containing residues in MetE or MetH and selenohomocysteine is a substrate for both enzymes, selenohomocysteine offers the opportunity to determine definitively whether the substrate binds directly to the zinc ion. In addition, by measuring XANES (X-ray absorption near-edge structure) and EXAFS at the Se edge, we have been able to characterize changes in the effective charge of the selenolate anion upon binding to MetE and MetH(2−649) and to determine the approximate geometry of the substrate-bound active site in both enzymes. Identification of the zinc ligands and the geometric changes at the zinc-binding site provides clues to the catalytic mechanism of methyl transfer in the methionine synthase enzymes.

MATERIALS AND METHODS

Expression and Purification of the MetE Protein. The recombinant substrate-free MetE enzyme was overexpressed by growing *E. coli* strain GW2531/pJG816 aerobically at 37 °C to late log phase or early stationary phase (A_{420} about 8.0) in Luria−Bertani medium supplemented with 100 μg/mL ampicillin, 0.5 mM zinc sulfate, and 0.4 mM isopropyl β-D-thiogalactopyranoside (IPTG) as previously described (*8*). The protein was purified by DEAE-Sepharose ion-exchange chromatography using a linear gradient of potassium phosphate buffer (180−500 mM at pH 7.2 containing 500 μM DTT) as previously described (*8*). Protein was purified to homogeneity as judged by electrophoresis in 12% polyacrylamide gels in the presence of sodium dodecyl sulfate (SDS−PAGE) and visualized by Coomassie blue staining. Purified protein was obtained with yields of ∼100 mg/L of growth medium, and was concentrated to about 100 mg/mL and stored at −80 °C.

Expression and Purification of MetH(2−649). Construction and characterization of the MetH(2−649) overexpression plasmid, pCWG02, have been described (*7*). However, a slightly altered enzyme purification method was used in this study. The cells were grown in Luria−Bertani medium supplemented with 100 μg/mL ampicillin, 0.5 mM zinc sulfate, and 0.4 mM IPTG. The cells were pelleted and sonicated as described previously, but no protease inhibitors were added to the sonicated cells. Only one column, an anion exchange Q-Sepharose gravity-flow column (Pharmacia), was used for purification. A linear gradient of 50−300 mM sodium phosphate buffer, pH 7.2, was used. MetH(2−649) can be purified to apparent homogeneity in a single chromotographic step due to the very high expression level of the fragment. Enzyme purity was determined by SDS−PAGE, and enzyme concentration was determined by a Bradford protein assay (Bio-Rad).

Preparation of Selenohomocysteine and Enzymatic Conversion to Selenomethionine. L-Selenohomocystine was synthesized from L-selenomethionine using sodium in liquid ammonia as described in detail elsewhere (*11*), and was reduced to L-selenohomocysteine immediately before use by incubation with tris(carboxyethyl)phosphine (TCEP). L-Selenohomocysteine has been shown to be a substrate for both MetE and MetH (*11*). With MetH, k_{cat}, determined using the methylcobalamin−homocysteine methyltransferase assay, is approximately 4 times faster for selenohomocysteine than for homocysteine, while with MetE, k_{cat} is about 50% that for homocysteine. In both cases, the K_m values for selenohomocysteine are similar to those for homocysteine: <125 μM for MetE and ∼15 μM for MetH.

XAS Sample Preparation. Substrate-free MetE and MetH(2−649) samples (∼3.3 mM) were equilibrated in 50 mM potassium phosphate buffer at pH 7.2. Selenohomocysteine was generated in situ immediately prior to each experiment, using a stoichiometric amount of TCEP (*12*). An excess (6 mM final concentration) of L-selenohomocysteine (SeHcy) was added to both the MetE and MetH samples to ensure saturation and therefore homogeneity of the zinc sites. For selenium XAS measurements, substoichiometric L-selenohomocysteine (2.4 mM final concentration) was used to ensure homogeneity of the selenium XAS signals. Upon addition of substrate, the samples were loaded into 150 μL Lucite cuvettes with 40 μm Kapton windows and frozen rapidly in liquid nitrogen. Additional samples of 20 mM SeHcy + 10 mM TCEP in 50 mM potassium phosphate buffer were prepared at pH 7.2 and pH 10 (to ensure deprotonation of the selenol) and 20 mM selenocystamine (obtained form Sigma) + 10 mM TCEP in 50 mM potassium phosphate buffer at pH 10 for use as references. These samples were also loaded into a Lucite cuvette and frozen rapidly in liquid nitrogen. Potassium tetrabromozincate was prepared via the method described by Jochum et al. (*13*). The crystalline K_2ZnBr_4 was diluted with boron nitride, ground into a fine powder, and packed evenly into a 0.5 mm aluminum sample cell with 40 μm Kapton windows.

XAS Measurements and Data Analysis. Zinc XAS data for substrate-free MetE and MetH were measured previously (*9*). Zinc XAS data were collected on two independent preparations of MetE + SeHcy, MetH(2−649) + SeHcy, and selenocystamine + TCEP at the Stanford Synchrotron Radiation Laboratory (SSRL) on beamline 9-3 using a fully tuned Si(220) double-crystal monochromator and a Rh-coated upstream mirror for harmonic rejection. Selenium XAS data for a single preparation of MetE + substoichiometric SeHcy and SeHcy + TCEP (pH 7.2) were measured under the same conditions. Se XAS data for separate preparations of MetE + substoichiometric SeHcy and MetH(2−649) + sub-

stoichiometric SeHcy and for a single preparation of SeHcy + TCEP (pH 7.2 and pH 10) were measured at SSRL on beamline 7-3 using a Si(220) double-crystal monochromator detuned to 50% of the maximum intensity for harmonic rejection. Additional selenium XAS data were collected on an independent preparation of MetH(2−649) + substoichiometric SeHcy at SSRL on beamline 2-3 using a Si(220) double-crystal monochromator detuned to 50% of the maximum intensity for harmonic rejection. The protein XAS data were collected as fluorescence excitation spectra using a Ge 13-element, solid-state detector array on beamlines 2-3 and 7-3 and a 30-element Ge detecor array on beamline 9-3. Measurements for both zinc and selenium were made using 10 eV increments in the preedge, 0.35 eV increments in the edge region, and 0.05 Å^{-1} increments in the EXAFS region with integration times of 1, 1, and 1−25 s (k^3-weighted), respectively, for a total scan time of ca. 35 min. Total integrated count rates were held below 90 kHz per channel to avoid saturation of the detector (Table S1 of Supporting Information). The windowed Zn Kα count rates and Se Kα count rates are given in Table S1. The total useful fluorescence counts per second per scan were 6.4×10^6 to 1.1×10^7 for the zinc spectra and 4.6×10^5 to 2.5×10^6 for the selenium spectra (Table S1). Zinc and bromine XAS data were collected at SSRL on beamline 2-3 using a Si(220) monochromator detuned to 50% of the maximum intensity for harmonic rejection. These data were measured using an N_2-filled ion chamber to measure the transmission through the sample. Transmission measurements for both zinc and bromine were made using 10 eV increments in the preedge, 0.35 eV increments in the edge region, and 0.05 Å^{-1} increments in the EXAFS region with integration times of 1, 1, and 1−15 s (k^3-weighted), respectively, for a total scan time of ca. 25 min. The temperature was held at 10 K during all of the measurements using an Oxford liquid helium flow cryostat.

All of the detector channels in each scan were examined individually for glitches, and the good channels (Table S1) were averaged for each sample to give the final spectrum. For the zinc measurements, the X-ray energies were calibrated by measuring the absorption spectrum of a zinc foil reference simultaneously with the fluorescence data and assigning the first inflection point in the zinc foil as 9659 eV. The selenium measurements were calibrated in a similar manner, using a selenium foil reference and assigning the first inflection point of the selenium foil spectrum as 12 658 eV. The bromine measurements were calibrated by simultaneous measurement of a $ZnBr_2$ foil and assigning the first inflection point as 13 474 eV.

Zinc, selenium, and bromine XANES data were normalized by fitting the data both below and above the edge to tabulated X-ray absorption cross sections (*14*) using a fourth-order polynomial and a single scale factor (*15*). The EXAFS background correction was performed by fitting a first-order polynomial to the preedge region, and a two-region cubic spline above the edge. After the background was removed, the data were converted to k-space using $k = [2m_e(E - E_0)/\hbar^2]^{1/2}$, where $E_0 = 9675$ eV in the case of zinc, 12 680 eV for selenium, and 13 500 for bromine. Fourier transforms were calculated using k^3-weighted data over the ranges given in Table S1 for both the zinc and selenium spectra. The first shell (Table S1) was then back-transformed over the same k-range. Both first-shell-filtered data and unfiltered EXAFS data were fit to eq 1 using a nonlinear, least-squares algorithm. Filtered and unfiltered data gave equivalent structural parameters.

$$\chi(k) = \sum_i \frac{N_i S_i(k) A_i(k)}{kR_i^2} \exp(-2k^2\sigma_i^2) \sin(2kR_i + \phi_i(k)) \quad (1)$$

EXAFS data are described by eq 1, where $\chi(k)$ is the fractional modulation in the absorption coefficient above the edge, N_i is the number of scatterers at a distance R_i, $A_i(k)$ is the effective backscattering amplitude, σ_i^2 is the root-mean-square variation in R_i, $\phi_i(k)$ is the phase shift experienced by the photoelectron wave in passing through the potentials of the absorbing and backscattering atoms, $S_i(k)$ is a scale factor specific to the absorber−scatterer pair, and the sum is taken over all scattering interactions (*16*). The program Feff v. 6.01 (*17*) was used to calculate the amplitude and phase functions, $A_i(k)$ and $\phi_i(k)$, respectively, for a zinc−oxygen at 2.00 Å, zinc−nitrogen at 2.05 Å, zinc−sulfur at 2.35 Å, zinc−selenium at 2.45 Å, selenium−carbon at 1.95 Å, selenium−sulfur at 3.60 Å, bromine−zinc at 2.40 Å, bromine−potassium at 3.60 Å, and bromine−bromine at 4.00 Å.

All of the fits were performed by allowing R and σ to vary for each shell while holding all of the other parameters fixed. Fits to the zinc spectra were calculated as described previously (*9*) with the zinc constrained to be either 4- or 5-coordinate with a variable ratio of nitrogen/oxygen, sulfur, and selenium. The selenium EXAFS for the substrate-bound enzymes was fit as a 2-coordinate selenium atom bound to carbon and zinc, varying the number of Se−S interactions in integer increments from 0 to the values of S_{max} determined previously ($S_{max} = 2$ for MetE and $S_{max} = 3$ for MetH) for the Zn sites in MetE (*8*) and MetH (*9*). The bromine EXAFS data were modeled, holding the coordination number fixed constant with the crystal structure and allowing R and σ to vary, for comparison with the parameters from the selenium spectra.

RESULTS

Selenohomocysteine Binds Directly to Zinc. Figure 1 shows the Fourier transforms of the zinc EXAFS data for MetE (bottom panel) and MetH(2−649) (top panel). It is evident that there is a progressive increase in the amplitude of the main peak on going from substrate-free enzyme to enzyme + homocysteine to enzyme + selenohomocysteine. The increase in amplitude alone could be caused either by a change in ligation (N/O to S to Se) or by a decrease in disorder when substrate binds. In addition to the increase in amplitude, there is a shift in the main peak to higher R. This shift to higher R is inconsistent with a more ordered site, and indicates instead a change in ligation. The changes in the Fourier transform are more pronounced for MetE than for MetH. This is consistent with the presence of more low-Z ligands in substrate-free MetE. The replacement of an O/N ligand with S or Se thus causes a greater percentage change in the EXAFS for MetE.

Quantitative fits to the EXAFS confirm these qualitative conclusions. The zinc EXAFS for enzyme + SeHcy (Figure 2) cannot be fit without including a Zn−Se shell. The fit

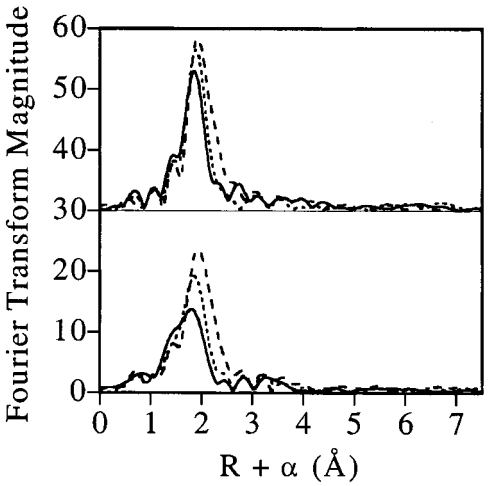

FIGURE 1: Representative Fourier transforms of the zinc EXAFS data from MetE (bottom panel) and MetH(2−649) (top panel) for the substrate-free enzyme (solid lines), enzyme in the presence of excess L-homocysteine (dotted lines) and enzyme in the presence of excess L-selenohomocysteine (dashed lines).

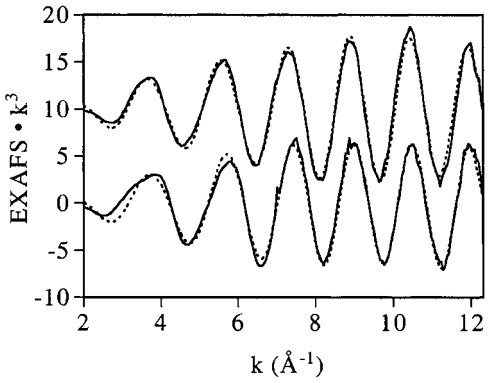

FIGURE 2: Representative Zn EXAFS data (solid lines) and fits (dotted lines) for MetE (bottom) and MetH(2−649) (top) in the presence of excess L-selenohomocysteine.

details are given in Table S2, and the best fits are summarized in Table 1. Since there are no other selenium atoms present in either MetE or MetH(2−649), these results demonstrate unambiguously that the selenium of selenohomocysteine, and thus by analogy the sulfur of homocysteine, displaces one of the low-*Z* ligands at the Zn active site.

This structural picture is confirmed by the Se EXAFS. The Fourier transforms of the Se EXAFS (Figure 3) for SeHcy bound to the protein are dominated by an intense peak at $R + \alpha \approx 2$ Å, attributable to Se−Zn scattering, together with a weaker Se−C peak at $R + \alpha \approx 1.5$ Å. Quantitative fits to the data (Table 1 and Figure 4) confirm this structural picture and, importantly, give Zn−Se distances in excellent agreement with those found in the Zn EXAFS.

Zinc Geometry in Substrate-Bound MetE and MetH(2−649). The selenium EXAFS data not only give additional evidence for the direct ligation of the selenohomocysteine to zinc in methionine synthase, but also provide a means for determining the geometry of the zinc site in substrate-bound methionine synthase. The Fourier transforms for SeHcy bound to either MetE or MetH show weak features at higher *R* ($R + \alpha \sim 3-3.6$ Å) (Figure 3). These are not seen in the Fourier transform of the EXAFS data for the selenohomocysteine amino acid alone (Figure S3). For MetE, these appear as two resolvable peaks at $R + \alpha \sim 3.0$ and 3.6 Å, while only a single broad peak with a maximum at $R + \alpha \sim 3.1$ Å is seen for MetH(2−649) + selenohomocysteine. In both cases, the outer-shell features are well modeled with a shell of sulfur atoms at ∼3.81 Å (Table 1). In neither case could the low-*k* EXAFS oscillations ($3\ \text{Å}^{-1} < k < 5\ \text{Å}^{-1}$ in Figure 4) be reproduced without including an outer shell of *S* scatterers in the fit, especially the minima at 4 and 5 Å^{-1} (Figure S4). The minimum at 4 Å is also more pronounced in the data for MetH(2−649) than that of MetE, consistent with the larger number of S zinc ligands in MetH(2−649). We, therefore, attribute this shell to Se••S scattering between SeHcy and the cysteines coordinated to the Zn.

Reports of intraligand EXAFS are relatively rare (*18*, *19*). To test the feasibility of detecting Se••S scattering, we measured Br EXAFS for the $ZnBr_4^{2-}$ anion. The tetrabromozincate anion has an approximately tetrahedral geometry, similar to that expected for methionine synthase, and is thus a good mimic for the expected behavior. The Fourier transform of the EXAFS data for $ZnBr_4^{2-}$ is included in the Supporting Information (Figure S5). As expected, there is a peak at $R + \alpha \sim 3.8$ Å, attributable to Br••Br scattering. There is, in addition, a peak at $R + \alpha \sim 3.2$ Å that is due to the K counterion in K_2ZnBr_4. All of the EXAFS distances for K_2ZnBr_4 (Table S4) are in excellent agreement with the crystallographic values (*13*). The split peak for MetE and the broad asymmetric peak for MetH(2−649) are due to interference between the scattering from the zinc at 2.43 Å and that from the sulfur atoms. The apparent number of sulfur atoms in the best fits, 2 for MetE and 3 for MetH(2−649), is consistent with the ligation predicted from earlier site-directed mutagenesis and EXAFS studies. The observed Se••S Debye−Waller factors are somewhat higher than those found for the Br−Br interaction in K_2ZnBr_4 (Table S4). This may reflect a small amount of disorder in the methionine synthase zinc sites.

By combining the Zn−Se, the Zn−S, and the Se−S distances, it is possible to calculate the average Se−Zn−S angle in the substrate-bound forms of MetE and MetH(2−649) (*18*). These angles are 106 ± 1° in MetE and 105 ± 1° in MetH(2−649) (Figure 5). These angles are consistent with slightly distorted tetrahedral zinc sites, supporting the 4-coordinate model used to fit the Zn EXAFS.

Zinc XANES Reflects Changes on Substrate Binding. Zinc XANES spectra (Figure 6) for both MetE and MetH(2−649) show that addition of either homocysteine or selenohomocysteine causes a small decrease in the intensity of the 9663 eV transition and a larger decrease in the intensity of the 9670 eV feature. In addition, the edge narrows upon addition of either substrate to either enzyme. The effects of substrate binding are shown more clearly in XANES difference spectra (Figure 7), calculated by subtracting the XANES spectra of the substrate-bound MetE and MetH(2−649) from the XANES spectra of the corresponding native enzymes. Perhaps the most striking feature of the Zn difference spectra is that homocysteine and selenohomocysteine cause nearly equivalent changes, particularly for MetE. Addition of either substrate gives pronounced negative features at ∼9662 and ∼9667 eV. Although there are differences between the different substrates and between the different enzymes, the negative features at ∼9662 and ∼9667 eV are apparent in all of the difference spectra.

Table 1: EXAFS Fitting Results for the Methionine Synthase Enzymes + L-Selenohomocysteine[a]

	shell 1			shell 2			shell 3		
	N	R_{ab} (Å)	$\sigma^2 \times 10^3$ (Å^2)	*N*	R_{ab} (Å)	$\sigma^2 \times 10^3$ (Å^2)	*N*	R_{ab} (Å)	$\sigma^2 \times 10^3$ (Å^2)
MetE (Zn)	1N	2.02(1)	2.7(1)	2S	2.33(1)	3.5(2)	1Se	2.433(1)	2.1(2)
MetH (Zn)	3S	2.36(1)	3.6(4)	1Se	2.430(2)	2.5(2)			
MetE (Se)	1C	1.981(3)	3(1)	1Zn	2.426(0)	2.7(3)	2S	3.80(2)	13(3)
MetH (Se)	1C	1.984(3)	3.3(7)	1Zn	2.433(5)	2.6(1)	3S		13(2)

[a] Parameters given are from fits to filtered data. Fits to unfiltered data gave similar structural parameters. Numbers in parentheses represent the reproducibility in the last digit, determined by examining multiple preparations of a single sample type.

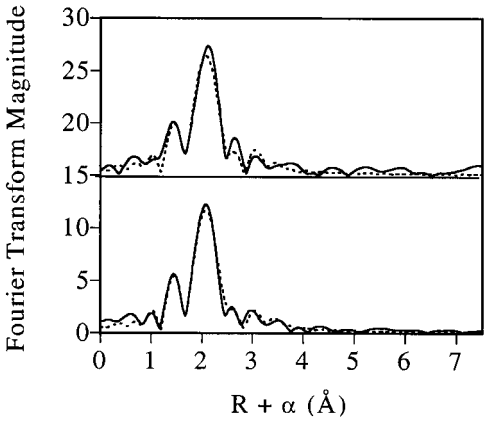

FIGURE 3: Representative Fourier transforms of selenium EXAFS data (solid lines) and best fits (dotted lines) from MetE (bottom) and MetH(2−649) (top) in the presence of substoichiometric L-selenohomocysteine.

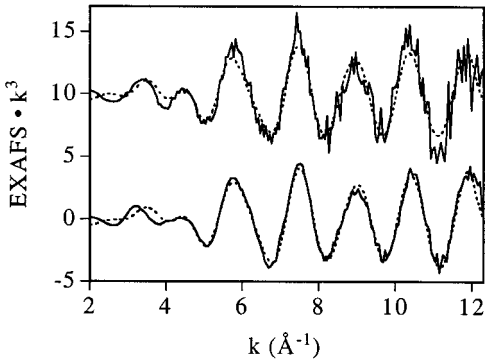

FIGURE 4: Representative Se EXAFS data (solid lines) and fits (dotted lines) for MetE (bottom) and MetH(2−649) (top) in the presence of substoichiometric L-selenohomocysteine.

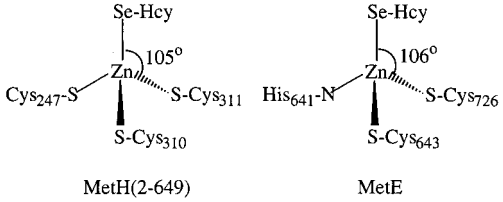

FIGURE 5: Proposed structure of the selenohomocysteine-bound Zn sites in MetH(2−649) and MetE. The amino acid ligands have been previously determined by site-directed mutagenesis (*6*, *8*−*10*). While stereochemistry is inferred in this scheme, there are no data available to assign the stereochemistry of these sites. The angles depicted in this scheme are the *average* Se−Zn−S_{Cys} angles.

The similarity of the XANES difference spectra following either SeHcy or Hcy binding is surprising. XANES spectra are generally considered to be, at least partially, determined by ligand identity. The observation of similar difference spectra, despite the differences in ligation [e.g., S_3(N/O) to S_4 vs S_3(N/O) to S_3Se], suggests that the difference features seen in Figure 7 reflect similar changes in the Zn site on binding of either substrate. In addition to the narrowing of the edge features, there appears to be a slight shift in the Zn edge to lower energy when either substrate binds. This appears as the negative feature at ~9662 eV. The slight shift of the edge to lower energy when either SeHcy or Hcy binds may reflect a small change in the effective charge on the Zn. Although the Zn remains formally Zn(II) in all cases, the binding of an anionic ligand and consequent decrease in the effective charge on the Zn would be expected to make excitation of the 1s electron slightly easier. While the shift in energy dominates the low-energy difference features in

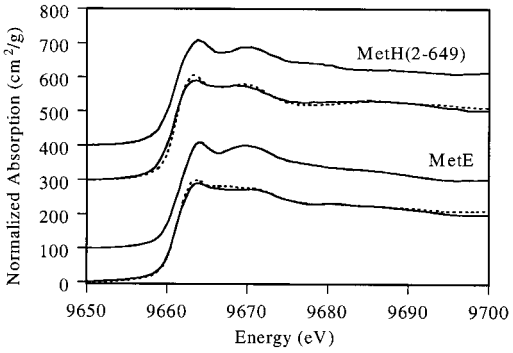

FIGURE 6: Representative zinc XANES spectra of MetH(2−649) (top three spectra) and MetE (bottom three spectra). XANES spectra for substrate-free enzyme are the first and fourth spectra from the top. The second, third, fifth, and sixth spectra are for enzyme plus excess L-homocysteine (solid lines) and for enzyme plus excess L-selenohomocysteine (dotted lines).

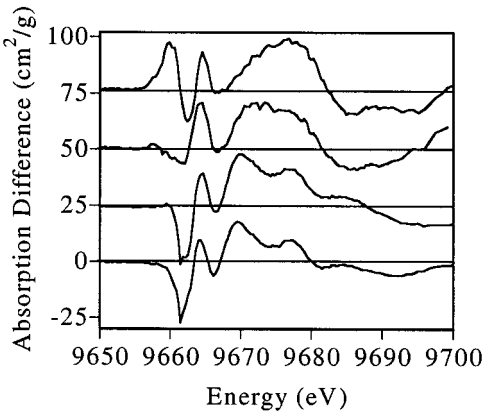

FIGURE 7: Representative zinc XANES difference spectra for (in order from top to bottom) MetH(2−649) plus excess L-selenohomocysteine, MetH(2−649) plus excess L-homocysteine, MetE plus excess L-selenohomocysteine, and MetE plus excess L-homocysteine. These spectra were calculated by subtracting the enzyme + substrate XANES spectrum from the substrate-free enzyme XANES spectrum. The difference spectra have been offset for clarity.

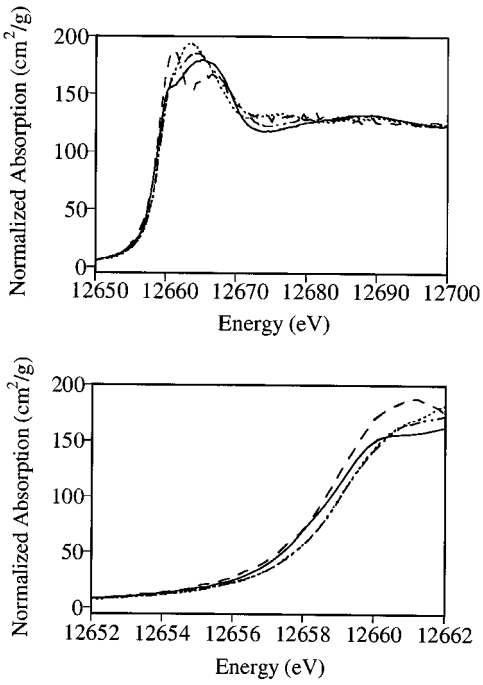

FIGURE 8: (Top) Selenium XANES spectra of selenohomocysteine + TCEP at pH 10 (solid line) and at pH 7.2 (dashed line), MetE in the presence of substoichiometric selenohomocysteine (dotted line), and MetH(2−649) in the presence of substoichiometric selenohomocysteine (dot−dashed line). (Bottom) The same spectra magnified to show the edge shift between the protein-free and protein-bound L-selenohomocysteine.

MetE, the MetH(2−649) difference spectra show more significant narrowing of the low-energy features. This is reflected in the derivative-shaped difference, which is more pronounced for the SeHcy than the Hcy-bound MetH(2−649). Determination of the Zn−S distance in the presence of SeHcy has shown that the increase in the average Zn−S distance when either substrate binds is, in fact, an increase in the Zn−S_{Cys} distance. This suggests that the narrowing of the substrate-bound Zn XANES spectra may be correlated with the increase in the average Zn−S_{Cys} distance.

Selenium XANES spectra for MetE + selenohomocysteine, MetH(2−649) + selenohomocysteine, and selenohomocysteine + TCEP at pH 7.2 and pH 10 are shown in Figure 8. The protein-free selenohomocysteine samples have similar edge energies and appear to have XANES features indistinguishable from previously published spectra of protonated and deprotonated selenocysteine (*20*). The two enzyme-bound selenohomocysteine spectra show small differences, suggesting there are differences in the selenium environments of MetE and MetH(2−649), consistent with their different Zn ligation. More striking, however, is the similarity of the edge energies for selenohomocysteine bound to either MetE or MetH. In both cases, the edge shifts by ∼0.7 eV to higher energy relative to protein-free selenohomocysteine at either pH 7.2 or pH 10. Since edge energy reflects, in part, the effective charge of the absorbing element (*21*), these results suggest that the interaction of the selenohomocysteine with either MetE or MetH(2−649) causes the effective charge on the Se atom to become less negative. This may reflect the Lewis acidity of the Zn^{2+} ion bound to the selenium atom of selenohomocysteine.

DISCUSSION

Many studies have demonstrated the efficacy of EXAFS as a tool for determining bond distances and types of ligands. However, the present study utilizes ligand EXAFS in combination with metal EXAFS to gain three-dimensional information about protein metal sites in solution. Coupling the three-dimensional information gained from the EXAFS with qualitative changes in the XANES can offer insight into how the changes taking place at the active site of metalloenzymes contribute to the overall turnover mechanism. In other members of this new class of zinc-dependent alkyl transferase enzymes, as in MetE and MetH, Se XAS may prove to be a valuable method for probing the catalytic role of zinc and the mechanism of alkyl transfer in the native enzymes.

The results presented herein provide definitive proof that the Se of selenohomocysteine, and by analogy the S of homocysteine, binds directly to the Zn ion in both MetE and MetH(2−649). The similarity of the Zn difference XANES spectra for both MetE and MetH(2−649) when excess homocysteine or excess selenohomocysteine is added shows that the S and the Se atom bind the Zn in a similar manner. This similarity, despite the difference in the ligands, indicates that there is a distinct change in the nature of the Zn ligand environment that has little to do with the ligand identity (i.e., S vs Se). While it is possible that some of the changes in the XANES, particularly those at higher energy, may be due to changes in geometry at the Zn site, the fact that the bond angles that are calculated for the substrate-bound enzyme show very little distortion from tetrahedral suggests that the Zn site does not suffer serious distortion.

The change in Zn XANES is explained, in part, by the increase in the average Zn−ligand distance when either Hcy or SeHcy binds. This increase, while small (0.02−0.03 Å), is significantly larger than the precision of the EXAFS (∼0.004 Å). Identical increases are seen for MetE and MetH. These small increases in the bond distance are expected to produce a slight narrowing of the edge spectra (*22*), and may account for the large positive difference between ∼9665 and ∼9668−9680 eV in the difference spectra. Lengthening of the Zn−S bonds upon substrate binding suggests that the ligand environment in the Zn is compensating for additional charge donation of the substrate (*23*). In addition to the sharpening of the edge, there is also a slight shift of the Zn edge to lower energy when Hcy or SeHcy binds. This can be seen in the negative difference feature at ∼9662 eV. Often, a shift to lower energy is associated with a decrease in oxidation state. For Zn(II), no such decrease is possible. However, it is possible that the small shift to lower energy reflects a small decrease in the effective charge on the Zn ion.

Charge donation from the substrate to the Zn ion is also seen in the shift to higher energy of the Se XANES spectrum of the protein-bound selenohomocysteine relative to that for the protein-free selenohomocysteine. While this shift (∼0.7 eV) is small compared with those observed for oxidation state changes, it is consistent with a slight decrease in the effective (anionic) charge on the Se due to interaction with a good Lewis acid (*24*). It was unexpected that the edge energy, and thus the degree of charge donation to the Zn in the resting state, would be identical in both MetE and MetH.

Model studies of zinc alkylthiolates have suggested that the reactive species is the free thiolate rather than the zinc-bound thiolate and have demonstrated that the greatest reactivity is seen with $(Zn[SR]_4)^{2-}$ complexes (*25*). We therefore expected that the selenium XANES spectrum of SeHcy bound to MetE, with a presumed net charge for the Zn center of −1, would be different from the spectrum of SeHcy bound to MetH with a net charge of −2. In fact, the spectra are very similar; from the perspective of the substrate, the Zn complexes of MetE and MetH look much the same. The Zn EXAFS results suggest that, in the absence of substrate, small bond length differences between the two clusters have already largely compensated for the differing net charges. On addition of either RS^- or RSe^-, further compensatory changes occur in each complex. These changes are reminiscent of the valence buffering seen in cytidine deaminase as the net charge of the Zn center changes during the catalytic cycle (*26*). One may speculate that the large and relatively rigid scaffold provided by the enzyme allows valence buffering, perhaps via hydrogen bonding that does not occur in small model complexes. The identical Zn−Se bond distances in MetE and MetH(2−649) suggest that these effects dominate any effects due to the net charge on the different Zn sites.

ACKNOWLEDGMENT

We thank the staff of SSRL for making this work possible. SSRL is supported by the Department of Energy, Office of Basic Energy Sciences. The SSRL Biotechnology Program is supported by the National Institutes of Health, National Center for Research Resources, Biomedical Technology Program, and by the Department of Energy, Office of Biological and Environmental Research.

SUPPORTING INFORMATION AVAILABLE

Supporting Information for this paper includes tables of the Zn and Se EXAFS fitting parameters for the methionine synthase enzymes and Br EXAFS fitting parameters for the K_2ZnBr_4 complex. Also included are figures showing the EXAFS data and best fits for all of the methionine synthase samples, the XANES and Fourier transforms of the L-selenohomocysteine and L-selenocystamine data with TCEP at pH 10, and the Br EXAFS data and Fourier transform of the K_2ZnBr_4 complex (9 pages). This material is available free of charge via the Internet at http://pubs.acs.org.

REFERENCES

1. Auld, D. S. (1997) in *Metal Sites in Proteins and Models: Phosphatases, Lewis Acids and Vanadium* (Sadler, P. J., Ed.) pp 29−50, Springer-Verlag, Berlin.
2. Goulding, C. W., and Matthews, R. G. (1997) *Curr. Opin. Chem. Biol. 1*, 332−339.
3. Hightower, K. E., and Fierke, C. A. (1999) *Curr. Opin. Chem. Biol. 3*, 176−181.
4. González, J. C., Banerjee, R. V., Huang, S., Sumner, J. S., and Matthews, R. G. (1992) *Biochemistry 31*, 6045−6056.
5. Banerjee, R. V., Frasca, V., Ballou, D. P., and Matthews, R. G. (1990) *Biochemistry 29*, 11101−11109.
6. Goulding, C. W., and Matthews, R. G. (1997) *Biochemistry 36*, 15749−15757.
7. Goulding, C. W., Postigo, D., and Matthews, R. G. (1997) *Biochemistry 36*, 8082−8091.
8. González, J. C., Peariso, K., Penner-Hahn, J. E., and Matthews, R. G. (1996) *Biochemistry 35*, 12228−12234.
9. Peariso, K., Goulding, C. W., Huang, S., Matthews, R. G., and Penner-Hahn, J. E. (1998) *J. Am. Chem. Soc. 120*, 8410−8416.
10. Zhou, Z. S., Peariso, K., Penner-Hahn, J. E., and Matthews, R. G. (1999) *Biochemistry 38*, 15915−15926.
11. Zhou, Z. S., Smith, A. E., and Matthews, R. G. (2000) *Bioorg. Med. Chem. Lett. 10*, 2471−2475.
12. Gunther, W. H. H. (1967) *J. Org. Chem. 32*, 3931−3933.
13. Jochum, M., Unruh, H.-G., and Barnighausen, H. (1994) *J. Phys.: Condens. Matter 6*, 5751−5760.
14. McMaster, W. H., Del Grande, N. K., Mallett, J. H., and Hubbell, J. H. (1969) U.S. Department of Commerce Report Number UCRL-50174-SEC 2-R1.
15. Waldo, G. S. (1991) Ph.D. Thesis, The University of Michigan, Ann Arbor.
16. Teo, B. K. (1986) *EXAFS: Basic Principles and Data Analysis*, Vol. 9, Springer-Verlag, New York.
17. Rehr, J. J., Albers, R. C., and Zabinsky, S. I. (1992) *Phys. Rev. Lett. 69*, 3397−3400.
18. Cramer, S. P., and Hille, R. (1985) *J. Am. Chem. Soc. 107*, 8164−8169.
19. George, G. N., Costa, C., Moura, J. J. G., and Moura, I. (1999) *J. Am. Chem. Soc. 121*, 2625−2626.
20. Pickering, I. J., George, G. N., Van Fleet-Stalder, V., Chasteen, T. G., and Prince, R. G. (1999) *J. Biol. Inorg. Chem. 4*, 791−794.
21. Myers, L. C., Jackow, F., and Verdine, G. L. (1995) *J. Biol. Chem. 270*, 6664−6670.
22. Bianconi, A. (1998) in *X-ray Absorption* (Konigsberger, D. C., and Prins, R., Eds.) pp 573−662, John Wiley and Sons, New York.
23. Brown, I. D., and Altermatt, D. (1985) *Acta Crystallogr. B 41*, 244−247.
24. Mande, C., and Sapre, V. B. (1982) in *Advances in X-ray Spectroscopy* (Bonnelle, C., and Mande, C., Eds.) pp 287−301, Pergamon Press, Oxford.
25. Wilker, J. J., and Lippard, S. J. (1997) *Inorg. Chem. 36*, 969−978.
26. Carlow, D. C., Carter, C. W. J., Mejlhede, N., Neuhard, J., and Wolfenden, R. (1999) *Biochemistry 38*, 12258−12265.

BI001711C